



Review

Modelling approaches in membrane distillation: A critical review

I. Hitsov^{a,b,*}, T. Maere^a, K. De Sitter^b, C. Dotremont^b, I. Nopens^a^aBIOMATH, Department of Mathematical Modelling, Statistics and Bioinformatics, Faculty of Bioscience Engineering, Ghent University, Coupure Links 653, 9000 Ghent, Belgium^bVITO – Flemish Institute for Technological Research, Boeretang 200, 2400 Mol, Belgium

ARTICLE INFO

Article history:

Received 27 August 2014

Received in revised form 22 December 2014

Accepted 24 December 2014

Available online 31 December 2014

Keywords:

Heat transfer

Mass transfer

Membranes

Simulation

Membrane distillation

ABSTRACT

Membrane distillation is a technique aimed at separating non-volatile components such as salts from aqueous feed streams. Mathematical modelling of a complex process like membrane distillation allows building further insight needed for effective analysis and optimization of the system, possibly leading to a breakthrough of the technology. Several models have been proposed in the literature for the heat and mass transport in the water channels of the module as well as inside the porous membranes. This article provides a critical review of these models and discusses the pros and cons of the different models to guide the reader into selecting the most suitable simulation approach. Moreover, research gaps in the literature are listed to indicate what is currently missing from a modelling as well as experimental data collection perspective. Areas for further research are suggested.

© 2015 Elsevier B.V. All rights reserved.

Contents

| | | |
|--------|---|----|
| 1. | Introduction | 49 |
| 2. | State of the art in membrane distillation modelling | 51 |
| 2.1. | Heat transfer models | 51 |
| 2.1.1. | General Nusselt number-based approach | 51 |
| 2.1.2. | Considerations and extensions of Nusselt equations HT models | 52 |
| 2.1.3. | Calculation of membrane thermal conductivity | 52 |
| 2.1.4. | Experimental validation of Nusselt equations HT model | 53 |
| 2.2. | Mass transfer (concentration polarization) inside the feed channel | 53 |
| 2.2.1. | Concentration polarization estimation based on the Sherwood number | 53 |
| 2.2.2. | Calculation of water partial pressure and activity | 53 |
| 2.3. | Models for mass transfer inside the membrane | 54 |
| 2.3.1. | Fick's law model | 54 |
| 2.3.2. | Dusty gas model | 54 |
| 2.3.3. | Simplifications of the DGM – Ordinary, Knudsen and Transition regions | 55 |
| 2.3.4. | Gas permeation test for evaluation of DGM membrane parameters | 55 |
| 2.3.5. | Limitations of the dusty gas model | 56 |
| 2.3.6. | Pore size distribution models | 56 |
| 2.3.7. | Schofield's model | 57 |
| 2.3.8. | Structural network models (Monte Carlo) | 57 |
| 2.3.9. | Ballistic transport model | 57 |

* Corresponding author at: BIOMATH, Department of Mathematical Modelling, Statistics and Bioinformatics, Faculty of Bioscience Engineering, Ghent University, Coupure Links 653, 9000 Ghent, Belgium.

E-mail addresses: Ivaylo.Hitsov@ugent.be (I. Hitsov), Thomas.Maere@ugent.be (T. Maere), Kristien.DeSitter@vito.be (K. De Sitter), Chris.Dotremont@vito.be (C. Dotremont), Ingmar.Nopens@ugent.be (I. Nopens).

| | | |
|--------|--|----|
| 2.4. | Empirical models | 57 |
| 2.4.1. | Artificial neural network (ANN) models | 58 |
| 2.4.2. | Empirical models based on tools from Design of Experiments (DoE) | 58 |
| 2.5. | Computational Fluid Dynamics (CFD) models | 58 |
| 2.5.1. | CFD models for heat transfer optimization in the channels | 59 |
| 2.5.2. | CFD models for heat and mass transfer optimization in the channels | 59 |
| 2.5.3. | CFD system models including the mass transfer inside the membrane | 59 |
| 3. | Discussion and research gaps | 60 |
| 3.1. | Discussion | 61 |
| 3.2. | Research gaps | 61 |
| 4. | Conclusions | 62 |
| | References | 62 |

Nomenclature

| | | | |
|--------------|---|-------------|--|
| \bar{P} | average pressure (Pa) | DCMD | Direct Contact Membrane Distillation |
| δ | membrane thickness (m) | DGM | Dusty Gas Model |
| ϵ | porosity (–) | DoE | design of experiments |
| γ | activity coefficient (–) | EE | Energy Efficiency (%) |
| κ | thermal conductivity (W/m K) | h | heat transfer coefficient (W/m ² K) |
| λ_i | mean free path of a the molecule (m) | H_v | specific heat of evaporation (J/mol K) |
| $ p_a _{ln}$ | logarithmic mean pressure of air across the membrane (Pa) | HT | Heat Transfer |
| μ | dynamic viscosity (Pa s) | K | mass transfer coefficient (m/s) |
| \bar{v} | mean molecular speed ($\sqrt{\frac{8RT}{\pi M}}$, m/s) | K_B | Boltzmann constant (m ² kg/s ²) |
| ρ | density (kg/m ³) | KTG | Kinetic Theory of Gasses |
| σ_i | water vapour collision diameter (Å) | m | molality (mol/kg) |
| τ | tortuosity (–) | MT | mass transfer |
| D | diffusive (superscript) | Mw | molar weight (kg/mol) |
| v | viscous (superscript) | N | flux (mol/m ² s) |
| a | air (subscript) | P | pressure (Pa) |
| b | bulk (subscript) | p | partial pressure (Pa) |
| f | feed (subscript, superscript) | P_a | average pressure of air inside the membrane (Pa) |
| g | gas (subscript) | Pr | Prandtl number (–) |
| m | membrane (subscript) | Pr_{wall} | Prandtl number at the membrane interface (–) |
| p | permeate (subscript, superscript) | q | heat flux (W/m ²) |
| s | solid (subscript) | R | universal gas constant (J/mol K) |
| w | water (subscript) | r | pore radius (m) |
| ANN | artificial neural network | Re | Reynolds Number (–) |
| c | concentration (mol/m ³) | RSM | response surface methodology |
| C_p | specific heat capacity (J/kg K) | SNM | Structural Network Model |
| CFD | Computational Fluid Dynamics | T | temperature (K) |
| D | diffusion coefficient (m ² /s) | U | overall heat transfer coefficient (W/m ² K) |
| d | characteristic size of channel (m) | v | velocity (m/s) |
| $D_{ij,e}^m$ | effective molecular diffusion coefficient (m ² /s) | VMD | Vacuum Membrane Distillation |
| D_{ij}^K | effective Knudsen diffusion coefficient (m/s) | x | molar fraction (–) |

1. Introduction

Membrane distillation (MD) was first developed in 1963 by Bodel when he patented the vapour diffusion through silicone rubber for saline water distillation [1]. The most used and studied MD configuration is the direct contact membrane distillation where the hot feed and the cold permeate solutions are separated by a hydrophobic membrane. The feed solution comes into contact with the membrane and evaporates, the vapour travels through the pores and condenses on the cold permeate membrane interface (Fig. 1).

The temperature difference across the membrane between the feed side (T_{mf}) and the permeate side (T_{mp}) as indicated in Fig. 1 results in different partial pressures of water vapour at the feed (P_{mf}) and the permeate side (P_{mp}). It is noteworthy that the actual driving force for the flux through the membrane is the vapour

pressure difference and only the evaporated phase is transported across the membrane. The use of thin membranes creates large vapour pressure gradients, therefore allowing MD to be operated at relatively low feed temperatures, potentially allowing to reuse waste heat from other processes.

The heat and mass transfer in MD are interconnected and lead to a complex relationship. When water is evaporated on the feed side it takes away part of the energy of the feed, which is carried away by the water vapour flux. This energy is transferred to the permeate during the condensation. Moreover, some of the energy is transferred through the membrane matrix itself via conduction in the form of sensible heat. The combined effect of the sensible heat and the heat due to evaporation creates thermal boundary layers near the interface of the membrane, leading to reduction of the intermembrane flux.

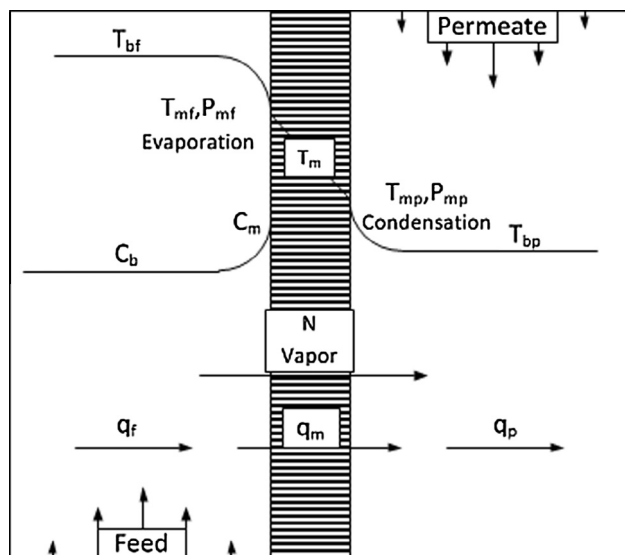


Fig. 1. Operation of direct contact membrane distillation.

Recently, it was attempted to directly measure the interfacial temperature using miniature PT100 sensors [2], but this method has the disadvantage that a special cell must be designed and the assumption that the sensors will not interfere significantly with the thermal boundary layers should hold. Another recent study measured the temperatures inside an MD module using Thermo-chromic Liquid Crystals (TLCs) [3,4]. The TLCs can be used to quickly and relatively accurately measure the temperature of a stream by recording the colour change [5]. Another approach is to model the system in order to predict the membrane temperatures. This could be done either using the semi-empirical Nusselt equations [6–9] which are frequently used in the design of heat exchangers, or by using the more physical approach of Computational Fluid Dynamics (CFD) [10–15], at the expense of larger computational power requirements. Both modelling approaches will be further discussed in this article and specific examples will be given.

There are four main contributions to the mass transfer inside the membrane pores: (1) molecular (ordinary) diffusion where the water vapours diffuse through the air trapped inside the larger pores of the membrane; (2) Knudsen diffusion occurs in the pores that have a size smaller than the length of the free path of the molecules for the given pressure and temperature; (3) viscous (poiseuille) flow is dominant in the larger pores in the cases where a total pressure difference across the pore exists; and (4) surface diffusion is a mechanism of molecule transfer on the surface of the membrane polymer, but is neglected in MD modelling, because it is expected that due to the hydrophobic nature of the membranes

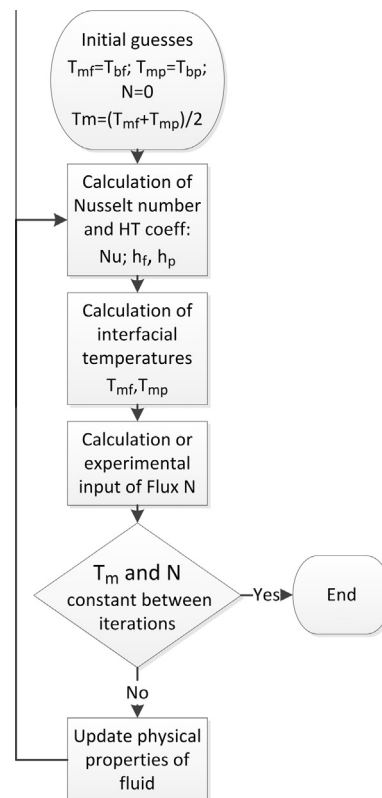


Fig. 2. Typical algorithm for simulation of MD using Nusselt equations for the water channels.

the molecule-surface interaction will be low [16]. Depending on the operational mode and the used membrane type, one or more of the transport mechanisms can be neglected in order to simplify the system model. The main models that deal with the vapour flow through the membrane are the Dusty Gas Model (DGM) [17–20], the Schofield's model [21,22], some applications of the Kinetic Theory of Gasses (KTG) applied for each pore in a distribution [9], as well as models that are applied based on flow in a network of interconnected pores mimicking the membrane structure [23–26]. When real solutions are used as feed instead of pure water the driving force will be lowered due to water activity reduction. Moreover, concentration polarization might occur, which additionally impairs the performance. This effect is strongest at high fluxes when the dissolved substance concentration near the membrane surface increases. The concentration polarization has not yet been directly measured but has been modelled either with a semi-empirical equation based on the Sherwood number or by CFD modelling.

Table 1
Comparative table of models available for membrane distillation.

| Name | Region | Type | Output | Physical |
|-------------------------------|--------------|-------------|-----------------------------------|----------|
| Nusselt equation | Channels | HT | T_{mf}, T_{mp}, TPC, EE | Semi |
| Sherwood equation | Feed Channel | MT | C_{mf} | Semi |
| Dusty gas model | Membrane | MT | N | Yes |
| Schofield's | Membrane | MT | N | Yes |
| Fick's | Membrane | MT | N | Yes |
| Structural network model | Membrane | MT | N | Yes |
| Kinetic theory of gasses | Membrane | MT | N | Yes |
| Ballistic transport model | Membrane | MT | N | Yes |
| Computational fluid dynamics | System | MT, HT | $N, \nabla T, \nabla v, \nabla c$ | Yes |
| Artificial neural networks | System | Black box | N, EE | No |
| Design of experiments toolbox | System | Statistical | System optimization | No |

An MD system allows for different operation modes such as feed temperatures, flow rates, concentrations, module configurations and membranes types to be incorporated. One could try to improve the performance of the system by varying the operational conditions in different modules, but this is an expensive and time-consuming job. Moreover, not fully understanding the transport mechanisms and phenomena occurring inside the system possibly results in one overlooking important parameters interactions. Therefore, it is crucial that MD is modelled in an accurate and physical way. A comparative table of the discussed models in this article is given in Table 1.

This article first describes these models in detail (Section 2). Section 3.1 then discusses and points out their pros and cons and finally Section 3.2 highlights current research gaps. As can be seen there are numerous models in the literature allowing to describe the different phenomena that are occurring in MD and often there are multiple models that can be used to simulate the same phenomenon and all have their strengths and limitations. This article is intended to help the reader gain process knowledge on membrane distillation and assist in choosing the best model for their particular simulation.

2. State of the art in membrane distillation modelling

2.1. Heat transfer models

2.1.1. General Nusselt number-based approach

Heat transfer models are used to describe and quantify the heat transfer in the vicinity of the membrane and predict the temperatures on the membrane interface. Heat transfer models also serve as a backbone for the mass transfer models by predicting the average temperature inside the membrane and the vapour pressure at the interfaces, which are needed as inputs for calculating the mass transfer. There are four contributions to the heat transfer process – (1) the heat transfer from the feed bulk to the membrane interface, (2) the heat flux through the membrane via conduction in the air/polymer matrix, (3) the heat transfer due to the flux of evaporated water and (4) the heat transfer from the permeate membrane interface to the bulk of the permeate channel. In equilibrated MD modules the heat flux in the water channels and the membrane must be equal (Eq. (1)).

$$\underbrace{h_f(T_{bf} - T_{mf})}_{(1)} = \underbrace{NH_v}_{(2)} + \underbrace{h_m(T_{mf} - T_{mp})}_{(3)} = \underbrace{h_p(T_{mp} - T_{bp})}_{(4)} \quad (1)$$

The symbols h_f , h_m and h_p represent the heat transfer coefficients of the feed, membrane and permeate, T , N and H_v the temperature, flux and specific heat of evaporation, respectively. The subscripts b , m , f and p represent the bulk, membrane interface, feed and permeate, respectively. Several heat transfer models have been developed in the literature for membrane distillation [2,7–9,27] but all are based on the calculation of the Nusselt number (Nu). In order to gain better understanding of these heat transfer models a schematic algorithm is given in Fig. 2. This algorithm is generic and the proposed models differ in the way certain steps are calculated. However, the used algorithm is always the same.

As a prerequisite for the calculation of Nusselt number, the Reynolds and Prandtl numbers must be calculated for the feed and the permeate channels. The mean membrane temperature is taken as an average of the bulk temperatures.

$$Re_{f,p} = \frac{vd\rho}{\mu} \quad (2)$$

$$Pr_{f,p} = \frac{\mu C_p}{\kappa} \quad (3)$$

In Eq. (2) Re , the Reynolds dimensionless number, represents a ratio of the inertial to viscous forces and is used to describe the hydrodynamic conditions of the flow. Pr in Eq. (3) stands for the Prandtl number, also dimensionless, representing the ratio of viscous to thermal diffusion rate. The symbols v , d , ρ , μ , C_p and κ represent the velocity, characteristic size of the geometry (diameter for a pipe and height for a channel), density, viscosity, specific heat capacity and thermal conductivity, respectively.

The next step is to evaluate the Nusselt number, a dimensionless number representing the ratio of the convective to diffusive heat transfer. Nusselt number are computed for the feed and permeate channels using the following correlation (Eq. (4)) valid for laminar regimes, given by Gryta et al. [6]:

$$Nu_{f,p} = 0.097 Re^{0.73} Pr_b^{0.13} (Pr_b/Pr_{wall})^{0.25} \quad (4)$$

The value of Pr_{wall} used in Eq. (4) is evaluated for fluid properties at the interfacial temperature of the feed or the permeate. It should be noted that the form of the Nusselt equation is unique to the channel geometry and the flow regime. Once the Nusselt numbers for feed and permeate are evaluated, the heat transfer coefficients of the feed and the permeate h_f , h_p can be obtained using the relation in Eq. (5):

$$h_{f,p} = \frac{Nu_{f,p} \cdot \kappa}{d} \quad (5)$$

The last step is to calculate the interfacial temperatures of the membrane, given by Khayet et al. [9].

$$T_{mf} = \frac{T_{bf} h_f + h_m \left(T_{bp} + T_{bf} \frac{h_f}{h_p} \right) - NH_v}{h_f \left(1 + \frac{h_m}{h_p} \right) + h_m} \quad (6)$$

$$T_{mp} = \frac{T_{bp} h_p + h_m \left(T_{bf} + T_{bp} \frac{h_p}{h_f} \right) + NH_v}{h_p \left(1 + \frac{h_m}{h_f} \right) + h_m} \quad (7)$$

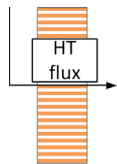
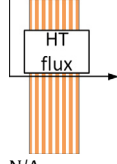
The above equations are derived from Eq. (1) assuming equality of heat flux in all compartments in steady state. The conductive heat transfer coefficient of the membrane h_m is determined as the ratio of the air/polymer matrix thermal conductivity κ_m and the thickness of the membrane δ

$$h_m = \frac{\kappa_m}{\delta_m} \quad (8)$$

It must be noted that the flux is included in the calculation of the interfacial temperatures (Eq. (6) and (7)). An initial guess for the

Table 2

Comparison of different models for the calculation of membrane thermal conductivity. Membrane parameters used: $\epsilon = 0.8$, polymer conductivity 0.25 W/(m K), gas conductivity = 0.027 W/(m K).

| Model | Graphical representation | Calculated κ_m (W/(m K)) |
|-----------|---|---------------------------------|
| Isostrain |  | 0.072 |
| Isostress |  | 0.033 |
| Maxwell I | N/A | 0.041 |

first iteration and later the flux from the previous iteration is used for current iteration. The algorithm is then restarted using the newly calculated interfacial temperatures and repeated until the difference in two consecutive calculated interfacial temperatures or fluxes are within a user-defined accuracy.

If the heat transfer model is used for experimental analysis (estimation of temperature polarization and membrane permeability), the flux from the experiments should be used.

2.1.2. Considerations and extensions of Nusselt equations HT models

Most of the authors [2,6–8,27] pay special attention to the choice of the Nusselt number correlation. The Nusselt number is a semi-empirical correlation used for the estimation of heat transfer coefficient in the water compartments. A commonly used form, valid for laminar flow MD modules [6] is given in Eq. (4). However, this form is not absolute and can greatly differ depending on the flow regime and module geometry. We must stress on the fact that the choice of Nu equation should be done very carefully. Usually, experimental data is collected and the experimental overall heat transfer coefficient is compared to the theoretical one in order to choose the best performing Nusselt equation. More information on the experimental validation of Nu number equations is given in Section 2.1.4. Extensive lists of Nusselt equations for different geometries can be found elsewhere [2,6–8,28].

The Nusselt equation predicts solely a uniform interfacial temperature, however in some cases an iterative procedure can be applied as done by Zhang et al. [29] where the geometry is split into a numbers of sections. The bulk temperature for each next segment is calculated by adjusting it with the exchanged energy of the previous elements using a heat balance. The procedure is stopped when the overall heat balance for the system is correct. By calculating the temperature for each section, the temperature profile along a MD module can be predicted. In order to validate the model, the flux is compared at different cell lengths and inlet temperatures. Excellent flux prediction was achieved in the validation. A similar approach was taken by Sirkar and Song [30], where a cross-flow, hollow fibre, direct contact MD module was simulated by splitting it into sections and adjusting the temperatures for each section using a heat balance. They also achieved good fit to experimental data. This is an alternative approach to using Computational Fluid Dynamics (CFD) for determining the flux and temperature distribution inside a module, but cannot be used to develop a novel spacer or fibre designs.

Another extension of HT models based on the Nusselt equation is proposed by Gryta and Tomaszewska to create a model that is non-isenthalpic with a non-linear temperature distribution inside the membrane [7]. The authors, however, do not explicitly state the significance of this addition. Phattaranawik et al. on the other hand [8] show that even though the intermembrane temperature is an exponential function of thickness, the temperature profiles are nearly linear due to the very thin membranes used in MD.

2.1.3. Calculation of membrane thermal conductivity

The thermal conductivity of the membrane is not easy to model as the matrix is comprised of a mixture of water vapour, air and polymer in a complex structure. Mainly two models are used in

the MD literature for the prediction of the thermal conductivity: the resistance in parallel model (Isostrain, Eq. (9)) [7,9,18,26,27,29,31,32] and the much less often used resistance in series model (Isostress, Eq. (10)) [8,33].

$$k_m = (1 - \epsilon)\kappa_s + \epsilon\kappa_g \quad (9)$$

$$k_m = \left[\frac{\epsilon}{\kappa_g} + \frac{1 - \epsilon}{\kappa_s} \right]^{-1} \quad (10)$$

In these equations κ_g and κ_s are the thermal conductivities of gas and polymer and ϵ is the porosity of the membrane.

It is noteworthy that both the series and the parallel models are limiting cases for possible membrane structures. The parallel model assumes a membrane which is ordered in such way that the polymer is oriented in the direction of the heat flux, whereas the series model assumes the gas/polymer layers to be evenly spaced and oriented in series, perpendicular to the heat flux (Table 2).

García-Payo and Izquierdo-Gil [33] performed an extensive evaluation of 9 different models for prediction of thermal conductivity of the membrane matrices of 2 PVDF, 2 PTFE and 2 supported PTFE membranes and compared them to experimental data. The authors concluded that the commonly used parallel model largely overestimates the thermal conductivity, whereas the series model slightly underestimates it. The best fit for all tested membranes and recommended to use for porosities higher than 60% was the Maxwell type I equation (Eq. (11)), where β is an intermediate factor.

$$\kappa_m = \frac{\kappa_g(1 + 2\beta(1 - \epsilon))}{1 - \beta(1 - \epsilon)} \quad (11)$$

$$\beta = (\kappa_s - \kappa_g)/(\kappa_s + 2\kappa_g) \quad (12)$$

Indicative κ_m predictions using these different modelling approaches are given in Table 2. This indicates that the resulting thermal conductivity very much depends on the choice of model, varying by a factor of 2 or more.

Zhang et al. [29] also commented on the choice of the thermal conductivity model and stated that the experimental measurement of highly porous membranes can be compromised by the force of clamping when using the experimental equipment. The authors noted that if the clamping force of the measuring equipment is too large, the membrane can collapse and the thermal conductivity will be overestimated due to the reduced porosity. On the other hand if the clamping force is too small the contact with the membrane will be insufficient and the conductivity will be underestimated.

Because of this uncertainty it is not possible to directly recommend the best model for predicting thermal conductivity. Generally it would be a safe choice to use the Maxwell Type I model as it is not developed for a limiting geometric case. Nevertheless, if the structure resembles the parallel (isostrain) model for example for a membrane produced with track etching or with photo lithographic methods where the pores are much less tortuous and more ordered, the use of the parallel model could be advisable.

A laser flash technique was used by Dumée et al. [34] to measure the thermal conductivity of the membrane. In this technique a laser pulse is applied on one side of the membrane and the

Table 3
Thermal conductivity of some polymers and linear fit equation coefficients, temperature in K.

| Polymer | Therm. cond., W/(m K) at 23 °C | Therm. cond., W/(m K) at 75 °C | Linear fit equation $\kappa = A \times 10^{-4}T_m + B \times 10^{-2}$ |
|------------------|----------------------------------|--------------------------------|---|
| PVDF | 0.17–0.19 [8] | 0.21 [8] | $A = 5.769$ $B = 0.9144$ |
| PTFE | 0.25–0.27 [8] | 0.29 [8] | $A = 5.769$ $B = 8.914$ |
| PP | 0.11–0.16 [8] | 0.20 [8] | $A = 12.50$ $B = -23.51$ |
| PES ^b | 0.145 ^a at 40 °C [37] | 0.16 ^a [37] | $A = 4.167$ $B = 1.452$ |

^a Graphical estimation from [37].

^b PES can be used in MD when modified to increase the hydrophobicity.

temperature response on the other side of the membrane is measured using an infrared detector. The authors coated both sides of the sample with thin gold and carbon layers. The gold layer was applied on the membrane to improve the surface thermal diffusivity and the carbon film was applied on top to minimize the laser reflection from the golden surface. The total reported coating thickness was 10 μm . This method is interesting for validation of thermal conductivity models, however it needs extensive sample preparation and care should be taken that the coatings adhere well to the membrane and do not alter its structure. Dumée et al. [34] also point out that a lower surface energy of the membrane can facilitate the formation of an air film adjacent to the membrane that further lowers the total conductive losses across the membrane. This effect has not been taken into account by any model to date.

The thermal conductivity of the air and water vapour trapped inside the pores is very similar and could thus be treated as one component [8,35]. Their thermal conductivity can be estimated based on the equation given by Jonsson et al. [32] (Eq. (13)) or alternatively by the more recent expression given by Bahmanyar et al. [36] (Eq. (14)).

$$\kappa_g = 1.5 \times 10^{-3} \sqrt{T_m} \quad (13)$$

$$\kappa_g = 2.72 \times 10^{-3} + 7.77 \times 10^{-5} T_m \quad (14)$$

The thermal conductivity of crystalline polymers is assumed to be a weak function of temperature [8], and some example values at 23 and 75 °C are given by Phattaranawik et al. [8] for PVDF, PTFE and PP. Additionally the thermal conductivity of PES can be graphically estimated from the work of Saleem et al. [37]. We derived an equation fit based on the assumption for linear change in conductivity as a function of temperature that could be used in modelling. A summary of the thermal conductivity of different polymers is given in Table 3.

2.1.4. Experimental validation of Nusselt equations HT model

In order to exclude the uncertainty the flux measurement and the uncertainty of the combined air and polymer thermal conductivity of the membrane (κ_m) some authors have proposed to use solid impermeable polymer sheets [7] or aluminium foil [8] in heat transfer experimental studies. The overall heat transfer coefficient U can be calculated from the measurement of inlet and outlet temperatures, flow rate F and the heat transfer area A .

$$Q = FC_p T_{in} - FC_p T_{out} \quad (15)$$

$$U = \frac{Q}{A \times LMTD} \quad (16)$$

Where $LMTD$ is the logarithmic mean temperature difference and Q is the heat flow calculated from the heat balance for one of the compartments. The experimental overall HT coefficient can be compared with the theoretical ones obtained by Eq. (5) using different Nu number correlations. The theoretical overall HT coefficient can be calculated using Eq. (17), and the advantage of using solid polymer or aluminium sheet instead of a membrane is the exact prediction of the term $\frac{\kappa_m}{\delta}$.

$$U = \frac{1}{\frac{1}{h_f} + \frac{\kappa_m}{\delta} + \frac{1}{h_p}} \quad (17)$$

2.2. Mass transfer (concentration polarization) inside the feed channel

As the salt is rejected at the membrane surface in the feed channel, the concentration near the membrane will increase. This phenomenon is known as concentration polarization. It is important to model this effect because it negatively influences the flux by reduc-

ing the water activity. Because MD achieves nearly 100% rejection for non-volatile components, the modelling is only required for the feed channel.

2.2.1. Concentration polarization estimation based on the Sherwood number

Similarly to the temperature polarization that happens inside the MD channels, concentration polarization will also occur in the feed channels of a module. In order to estimate the influence of this phenomenon Martínez-Díez and Vázquez-González [38] built a model for a flat sheet geometry that included the semi-empirical relations for the mass transfer in the channels based on the Graetz-LéVêque definition of the Sherwood number (Sh). The Sherwood number is a dimensionless number, the mass transfer equivalent of the Nusselt number representing the ratio of the convective to diffusive mass transfer:

$$c_{mf} = c_{bf} e^{Mw \cdot N / \rho K} \quad (18)$$

$$K = \frac{ShD}{d_h} \quad (19)$$

$$Sh = 1.86 \left(ReSc \frac{d_h}{L} \right)^{0.33} \quad (20)$$

$$Sc = \frac{\mu}{\rho D} \quad (21)$$

where Mw , c_{mf} , c_{bf} , K , D , Sc and L are the molar weight of water, concentrations at the membrane interface and bulk of the feed, the overall mass transfer coefficient, diffusion coefficient and the length of the geometry, respectively. Martínez-Díez et al. concluded that the interfacial salt concentration is as much as 4 percent higher compared to the bulk concentration [38] in the tested conditions with fluxes up to 10 kg/(m² h) and resulting driving force decrease of only 0.2%. In terms of driving force reduction, the concentration polarization in MD has a negligible contribution for low concentrations (see Fig. 3). This is shown by Martínez and Rodríguez-Maroto [20], where the heat and mass transfer resistances in a DCMD system are split and the resistance associated with concentration polarization becomes significant only for concentrations approaching saturation. Therefore, it would be safe to neglect the concentration polarization at low concentrations such as sea water. However, the concentration polarization is generally easy to model and does not add much computational burden and the models that include the concentration polarization phenomenon could be used to investigate the possibility of scaling on the membrane interface. Different modelling attempts for scaling [39], fouling [40–43] and biofouling [44] processes in MD exist in the literature, but are considered outside the scope of this review.

Similar to the Nusselt number, there is no universal form of the Sherwood Eq. (20) and its form depends on the flow regime and the geometry of the system. Most MD authors assume the analogy between the heat and mass transfer in the channels [8,38,45] with Sh and Sc numbers being the mass transfer equivalents of Nu and Pr numbers respectively. This analogy could be used to choose a Sherwood number equation after experimental validation of the Nusselt equation [38]. While there are attempts made to validate the interfacial temperatures with sensors [2] and thermochromic liquid crystals [3,4], no work is present in the literature that attempts to validate concentration polarization effects. An alternative to estimate the interfacial concentration is a study with CFD (see Section 2.5), although further validation would still be needed.

2.2.2. Calculation of water partial pressure and activity

To link the heat transfer models with the mass transfer model the partial pressure of water vapour must be calculated based on the interfacial temperatures. This can be done with the Antoine equation (Eq. (22)) [46]:

$$p_0 = \exp\left(23.5377 - \frac{4016.3632}{T - 38.6339}\right) \quad (22)$$

The above equation calculates the vapour pressure for pure water p_0 in Pa based on temperature T in Kelvin. However, when real solutions are used as feed, the water vapour pressure on the feed side is lowered due to the reduced water activity. The actual vapour pressure p_i can be recalculated using either the activity a_w , or the activity coefficient γ_i and the water mole fraction x_w [47].

$$p_i = p_0 a_w = p_0 x_w \gamma_i \quad (23)$$

The activity and the activity coefficients of water are used to represent the non-ideality of the solution. It is generally accepted that the calculated vapour pressure using Antoine's equation only differs on the feed side, as the permeate of MD is usually pure water. In MD literature a fit to the experimental data derived by Schofield et al. [48] is cited in order to calculate the activity coefficient of the water-salt mixture [19,49].

$$\gamma_i = 1 - 0.5x_{\text{NaCl}} - 10x_{\text{NaCl}}^2 \quad (24)$$

Other references where the water activity could be obtained were compared to the one calculated with Eq. (24) (Fig. 3).

As can be seen in Fig. 3, the activity obtained from the empirical equation of Schofield (Eq. (24)) [48] (seen as dashed line) slightly deviates from the referenced experimental data, in the sense that it underestimates the activity at high concentrations. Because of the discrepancies using Eq. (24), we propose a second order polynomial fit to the data and the prediction of this new equation is seen as solid line (Fig. 3). The experimental data used to make the polyno-

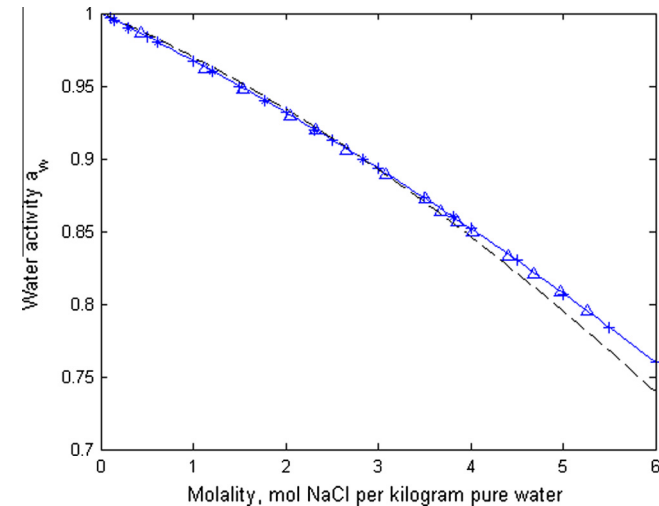


Fig. 3. Water activity in salt solutions obtained from different sources. Legend: “+” [50] at 25 °C, “*” [51] at 25 °C, “△” adapted for molality from [52] at 35 °C, dashed line adapted for activity and molality from – Eq. (24), solid line fit using Eq. (25).

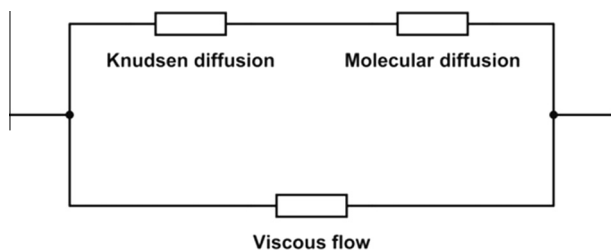


Fig. 4. Schematic representation of DGM.

mial fit was taken from the latest water activity reference from 2007 [50] where the salt concentration was varied from 0 all the way until saturation. The newly proposed equation is given below:

$$a_w = 1 - 0.03112m - 0.001482m^2 \quad (25)$$

where m is the NaCl molality (mol NaCl per kilogram pure water). The activity of water also depends on the temperature of the solution, although this effect is small [51]. In the article of Chirife and Resnik [53] the difference in activities of salty water between 25 and 60 °C is less than 0.2%, indicating that there is no need for a temperature correction for salt solutions. More examples of equation fits for different solutes are given by Khayet and Matsuura [49]. However, if a more complex mixture of ions is used as feed, more sophisticated and physical models such as the Pitzer's equations [54] or the non-random two-liquid (NRTL) [55] model must be used to predict the water activity.

2.3. Models for mass transfer inside the membrane

Numerous models used to describe the mass transfer of water vapour inside the porous MD membrane exist in the literature. One of the simplest ways is to use Fick's law that treats the membrane as an empty space full of air in which the molecules of the water vapour are diffused. This approach does not consider the membrane structure such as the porosity, tortuosity and the pore size. These membrane parameters are taken into account for the much more widely used Dusty Gas Model and the Schofield's model. The latter models, however, do not take into account the effect of pore size distribution and an average pore size is used. Pore size distribution models have been developed based on the Kinetic Theory of Gases (KTG) and extensions of the Dusty Gas Model. Finally, a three dimensional model based on the KTG has been developed in order to simulate the effect of the pore size distribution and interconnectivity. In this section the different models are presented and discussed giving their pros and cons.

2.3.1. Fick's law model

One of the simplest ways to describe the mass transfer through the membrane region is by using the Fick's law model. By representing the membrane region as a space full of stagnant air, Bahmanyar et al. [36] uses an expression for the flux of the water vapours diffusing through the air (Eq. (26)–(29)).

$$N_{calc} = \frac{PM_w D_{w-a}}{RT_m \delta} \ln \frac{P - p_{mp}}{P - p_{mf}} \quad (26)$$

$$D_{w-a} = \frac{2.634}{P} \left(\frac{T_m}{273.15} \right)^{1.5} \quad (27)$$

$$D_{eff} = \frac{N_{exp}}{N_{calc}} D_{w-a} \quad (28)$$

$$N_{eff} = \frac{PM_w D_{eff}}{RT_m \delta} \ln \frac{P - p_{mp}}{P - p_{mf}} \quad (29)$$

The author first obtains an initial theoretical flux N_{calc} (Eq. (26)) using the theoretically calculated diffusion coefficient D_{w-a} (Eq. (27)). To calibrate the model, the theoretical diffusion coefficient D_{w-a} is multiplied with the ratio of the experimental N_{exp} and initially calculated N_{calc} fluxes to find the effective diffusion D_{eff} (Eq. (28)), which is subsequently used to calculate the effective flux N_{eff} (Eq. (29)).

2.3.2. Dusty gas model

Another way to describe the mass flow inside the membrane is the Dusty Gas Model (DGM) [56]. It can be applied for a multi-component mixture of gases, where the pores of the medium are represented as stationary pseudo gas molecules with large size

(dust) [57]. The effect of viscous (poiseuille) flow, as well as molecular and Knudsen diffusion are frequently modelled in porous media using the DGM [58,18,41]. Although theoretically the model can consider the effect of surface diffusion [17,59] it is generally considered negligible in the MD process [19] and has never been included in the MD modelling to our knowledge.

In its most general form the DGM equation used in membrane distillation is given by Lawson and Lloyd [19]. This model accounts for the flux due to molecular and Knudsen diffusion as well as viscous flow, but neglects surface diffusion [16,18] (Eq. (30)–(33)).

$$\frac{N_i^D}{D_{ie}^D} + \sum_{j=1}^n \frac{p_j N_j^D - p_i N_j^D}{D_{ije}^D} = \frac{-1}{RT} \nabla p_i \quad (30)$$

$$N_i^V = \frac{-p_i B_0}{RT\mu} \nabla P \quad (31)$$

$$N_i = N_i^D + N_i^V \quad (32)$$

$$D_{ij,e}^m = K_1 P D_{ij}, \quad D_{ie}^k = K_0 \sqrt{\frac{8RT}{\pi M_i}} \quad (33)$$

In the above equations N_i^D , N_i^V and N_i are the diffusive, viscous and total fluxes; P and μ are the total pressure and viscosity of the mixture while p_i is the partial pressure of component i , respectively. Finally, $D_{ij,e}^m$, D_{ie}^k represent the effective molecular and Knudsen diffusion coefficients and M_i is the molar weight of component i .

There are three constants (B_0 , K_0 , K_1) that depend on the membrane structure and are best determined experimentally due to the complex membrane structure [19]. As a quick approximation they can also be calculated using membrane parameters such as membrane pore radius, tortuosity and porosity (r , τ , ϵ) [19]:

$$B_0 = \frac{\epsilon r^2}{8\tau}, \quad K_0 = \frac{2\epsilon r}{3\tau}, \quad K_1 = \frac{\epsilon}{\tau} \quad (34)$$

It is generally accepted that during certain operational conditions some of the transport mechanisms can be excluded and some simplifications of the DGM are given in Section 2.3.3.

2.3.3. Simplifications of the DGM – Ordinary, Knudsen and Transition regions

The first simplification of the dusty gas model is the exclusion of the term $p_j N_j^D$ from Eq. (30), by assuming that the diffusive flux of air N_j^D is totally impaired by the low diffusion coefficient of air in water [19] and the low solubility of air in water [49].

An important characteristic of the vapour permeation process is the Knudsen number (Kn) which represents the relation of the mean free path that the molecule travels (λ) to the pore size of the membrane (d_p) expressed as $Kn = \lambda/d_p$. The mean free path of the molecule can be calculated using the equation:

$$\lambda_i = \frac{K_B T}{\sqrt{2} \pi \bar{P} \sigma_i^2} \quad (35)$$

In the equation above σ_i is the collision diameter, which is 0.2641 nm for water vapours [60]. K_B , T and \bar{P} respectively stand for the Boltzmann constant, the absolute temperature and the mean pressure in the membrane pores [16].

There are three main mass transport regimes that can be distinguished based on the Knudsen number. If $Kn > 1$ the molecules will collide mainly with the pore walls and therefore the Knudsen diffusion mechanism will be prevailing for the membrane pores and Eqs. (30)–(33) simplify to (36), by replacing the gradients of pressure ∇p_i with $\frac{\Delta p_i}{\delta}$ and neglecting the flux of air N_j . If the pore size is much larger than the mean free path of the water molecules ($Kn < 0.01$), the dominating transport mechanism will be molecular diffusion of water vapour through the stagnant air trapped inside the pore. This is described by Eq. (37), where $|p_a|_{ln}$ is the

log mean air pressure across the membrane [19]. Finally, a transition region exists for pore sizes characterized by $0.01 < Kn < 1$. Here, the transport will be governed by both molecular and Knudsen diffusion (Eq. (38)). The total flux equations for different permeation regimes as a function of the Kn number for a uniform pore size distribution are given by:

$$N^K = K_0 \frac{\bar{v}}{RT} \frac{p_{mf} - p_{mp}}{\delta}, \quad Kn > 1 \quad (36)$$

$$N^D = \frac{D_{ij,e}^m}{RT\delta} \frac{p_{mf} - p_{mp}}{|p_a|_{ln}}, \quad Kn < 0.01 \quad (37)$$

$$N^T = \frac{D_{ij,e}^m}{\delta RT} \ln \left(\frac{p_a^D D_{ie}^K + D_{ij,e}^m}{p_a^f D_{ie}^K + D_{ij,e}^m} \right), \quad 0.01 < Kn < 1 \quad (38)$$

where \bar{v} is the mean molecular velocity, $\sqrt{\frac{8RT}{\pi M}}$. In case there is a total pressure difference across the membrane, the viscous flow could easily be added as the DGM considers the viscous flow as a linear addition to the flux from molecular and Knudsen diffusion fluxes (Fig. 4). Typical cases where the viscous flux is combined with Knudsen are the vacuum membrane distillation using a membrane with larger pores, gas permeation and deaerated DCMD distillation [28,61] as described by Eq. (39):

$$N^{V-K} = \frac{1}{RT\delta} \left(D_{ie}^K + \frac{\bar{P} B_0}{\mu} \Delta P \right) \quad (39)$$

2.3.4. Gas permeation test for evaluation of DGM membrane parameters

Experimentally, the values of K_0 and B_0 can be estimated via gas permeation tests. Water vapours cannot be used because of condensation problems inside the test apparatus [19,62]. However, N_2 and CO_2 can be used successfully because the structural parameters as defined by DGM are independent of the used gas (Eq. (40)). The gas is pumped through the membrane and the pressures and fluxes are logged. The DGM equation for Knudsen-Poiseuille transition is rearranged in the form [19,46,63]:

$$\frac{NRT\delta}{\bar{v}\Delta P} = K_0 + B_0 \frac{\bar{P}}{\mu\bar{v}} \quad (40)$$

and the membrane structural parameters are evaluated from a linear fit of the experimental data, where K_0 is the intercept and B_0 is the slope. A simple mathematical transformation reveals the values of the pore radius and the coefficient K_1 :

$$r = \frac{16B_0}{3K_0}, \quad K_1 = \frac{3K_0}{2r} \quad (41)$$

A drawback of this type of gas permeation tests is that the membranes commonly used for membrane distillation are highly porous and the possibility exists that the membrane partially collapses at high transmembrane pressures [29]. An alternative gas permeation method for the determination of K_0 and B_0 is given by Lei et al. [64] and Zhang et al. [29,65], where the transmembrane pressure is kept constant at 1 kPa and the average pressure inside the membrane pores is varied. This alternative gas permeation experiment has the advantage of excluding the possibility of membrane compressibility due to the much lower applied transmembrane pressures.

Eq. (40) is derived for a flat sheet experiment. In case the tested membrane is cylindrical (hollow fibre or capillary) an equation derived for this geometry can be found in the work of Guijt et al. [62].

Zhang et al. also derived an experimental procedure for the evaluation of the permeability of hollow fibre membranes [66]. The authors used constant, low transmembrane pressure and varied the average pore pressure (by lowering or increasing the pressure simultaneously on both sides of the membrane). The obtained permeability parameters varied at different hollow fibre lengths

which was explained by the pressure drop along the membrane lumen. Therefore, the permeability was measured at different membrane lengths and extrapolated to zero length. The obtained parameters were later used to simulate a vacuum MD and the model proved to have high predictive power.

Lawson et al. [67] and Zhang et al. [29] proposed that under certain operational conditions some of the membranes used for MD can be compacted. As the membrane compacts the thickness is reduced which should increase the flux. Meanwhile, the compaction also increases the tortuosity and decreases the porosity and pore size, which has negative impact on the flux [67]. Lawson et al. [67] derived an expression to compensate these changes and noted a region where the permeability is increased by compaction, followed by a region of reduced permeability at higher compaction for a PP membrane. Zhang et al. [29] on the other hand only notices a negative effect from the compaction of PTFE membrane used in DCMD as the flux is reduced in the compressed membranes. Moreover, Zhang et al. noticed an increase in the membrane thermal conductivity at higher flow rates, which he attributed to the reduced porosity [29]. The membrane compaction effects are not taken into account in the majority of MD models and further investigation into these effects could be interesting for the community.

2.3.5. Limitations of the dusty gas model

The DGM is in fact derived for isothermal conditions, whereas in reality the temperature throughout the membrane is not constant [19]. Nevertheless, it has been successfully applied in membrane distillation using an average temperature for the membrane [16,19].

Recently the schematic representation of resistances in DGM has been questioned by Field et al. [68]. The model considers a resistance in series approach to Knudsen and molecular diffusions, with viscous flow in parallel (Fig. 4).

Field et al. argue that it is not physically possible to have Knudsen and viscous flow occurring in the same pore (Eq. (39) in this work). The authors point out that viscous flow occurs differently when the pore size is comparable to the mean free path of the molecules. Moreover, a new equation for the addition of Knudsen and molecular diffusion is proposed for the transition region [68]. New modified equations to include these arguments were presented and tested against experimental work, but the model was not calibrated and the goodness-of-fit of the new model was not estimated. It would be interesting to see more work that further elaborates this approach.

2.3.6. Pore size distribution models

Models that take into account the pore size distribution for MD membranes have been developed by Phattaranawik et al. [69] and Khayet et al. [9]. The authors split the contribution of the Knudsen, molecular and transition mechanisms by proposing an equation for each region based on the calculated Knudsen number. Phattaranawik and co-workers propose an equation with average pore size in each region based on the Dusty gas model, while Khayet and co-workers calculated the flux for each pore in the size distribution based on the Kinetic Theory of Gasses (KTG) for straight cylindrical non-interconnected pores. The governing equations representing the permeability of a single pore with an area of πr^2 for these three regions is given by Khayet [16]

$$B_i^K = \frac{2\pi}{3} \frac{\bar{v}}{RT} \frac{r_k^3}{\tau\delta} \quad Kn > 1 \quad (42)$$

$$B_i^D = \frac{\pi}{RT} \frac{PD_i}{p_a} \frac{r_d^2}{\tau\delta} \quad Kn < 0.01 \quad (43)$$

$$B_i^T = \frac{\pi}{RT} \frac{1}{\tau\delta} \left[\left(\frac{2}{3} \bar{v} r_t^3 \right)^{-1} + \left(\frac{PD_i}{p_a} r_t^2 \right)^{-1} \right]^{-1} \quad 0.01 < Kn < 1 \quad (44)$$

In Eq. (42) r_k , M_i and δ represent the pore size in the Knudsen region, molecular weight of species i and thickness of the membrane respectively. In Eq. (43) D_i is the diffusion coefficient, P and p_a the total and the air pressure inside the pore and r_d the pore size in the diffusion region. In Eq. (44) r_t is the pore radius in the transition region. Because of the fact that most membranes have a pore size distribution this means that usually more than one transport mechanism will govern the process.

Based on Eq. (42)–(44) Khayet et al. proposed an equation that could calculate the membrane flux for a distribution, instead of a uniform pore sizes [9]. In the resulting model the total membrane permeability is given by the following equations:

$$B_i^m = \frac{N}{\delta} \left[\sum_{j=1}^{m(r=0.5\lambda)} G_i^K f_j r_j^3 + \sum_{j=m(r=0.5\lambda)}^{p(r=50\lambda)} \left(\frac{1}{G_i^K r_j} + \frac{1}{G_i^D} \right)^{-1} f_j r_j^2 + \sum_{j=p(r=50\lambda)}^{n(r=r_{max})} G_i^D f_j r_j^2 \right] \quad (45)$$

$$G_i^K = \left(\frac{32\pi}{9M_i RT} \right)^{1/2} \quad (46)$$

$$G_i^D = \frac{\pi}{RT} \frac{PD_i}{p_a} \quad (47)$$

$$N = \frac{\epsilon/\tau}{\sum_{j=1}^n f_j \pi r_j^2} \quad (48)$$

where N , G_i , f are the number of pores per unit area, an intermediate term, and fraction of pores in this particular size class. The symbols m , n and p denote the largest pore size within each of the classes, i.e. Knudsen diffusion, Knudsen-molecular transition and the maximum pore size, respectively.

The authors of both pore size distribution models conclude that the influence of pore size distribution is not large and a single average pore size is an adequate representation [9,69]. Khayet and co-workers however state that this is due to the uniform pore size distribution of commercial membranes but potential discrepancies with the traditional method (mean pore size models) can be observed for membranes with a large standard deviation of pore size [9].

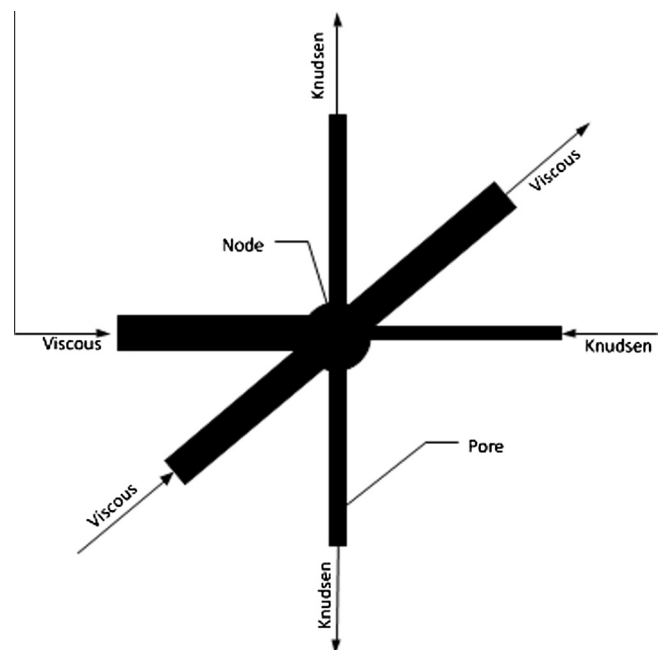


Fig. 5. Representation of a single node with pores in structural network models (figure reproduced from Imdakm et al. [25]).

2.3.7. Schofield's model

Schofield and co-workers [21,22,70] proposed the following semi-empirical approximation of the flux in the viscous-Knudsen transition region.

$$N = a\eta^b \Delta P \quad (49)$$

With η a dimensionless pressure equal to P/P_{ref} . The reference pressure is chosen as a typical pressure for the operation range, in order for η to be close to 1. Parameter a is the membrane permeation constant and b the contribution of viscous flow to the total flux (0: Knudsen controlled, 1: fully viscous flow) [22]. Eq. (49) is valid for deaerated systems and in order to account for the diffusive flux of water vapour in the air trapped inside the membrane pores, Schofield et al. proposed the following equation [22]

$$N = \left(\frac{1}{a\eta^b} + \frac{p_a}{d} \right)^{-1} \Delta P \quad (50)$$

$$d = \frac{\epsilon DPM}{\tau \delta RT} \quad (51)$$

As a first approximation of the coefficients a and b the following equations are proposed [21]:

$$a = M\bar{v}(A + BP_{ref}/L)/\delta \quad (52)$$

$$b = (BP_{ref}/L)/(A + BP_{ref}/L) \quad (53)$$

$$A = \frac{2r\epsilon}{3\tau RT} \quad (54)$$

$$B = \frac{\pi r^2 \epsilon}{32\tau RT} \quad (55)$$

A disadvantage of the Schofield's model, as pointed out by Lawson and Lloyd [19] and Fernández et al. [46] is the dependency on the gas used to perform the permeability tests and the large experimental error that is associated with the determination of the coefficients a and b in Eq. (49). An extensive comparison between the Schofield's model and the Dusty gas model was performed by Fernández et al. [46] and concluded that the DGM is superior to the Schofield's model and DGM was recommended as "the more physical" approach.

2.3.8. Structural network models (Monte Carlo)

In essence, what is characteristic to these models is the 3D network of pores and nodes used to represent the membrane structure. The first structural model for membrane distillation was published by Imdakm and Matsuura [23] in 2004, where the authors applied the model to simulate 3 hypothetical membranes. A Monte Carlo method was applied to map the pore size distribution to a structure of nodes interconnected with pores, making the authors refer to them as Monte Carlo Models. However, we would like to point out that Monte Carlo is a general term for a methodology for system simulation where samples are taken randomly from a defined input distribution, solved through a model function which results in an output distribution of solutions [71].

Hence, the term Monte Carlo should not be used to represent a class of models. We therefore propose to more correctly refer to these models as Structural Network Models (SNM). A building block (single node) of these models is shown in Fig. 5.

In order to represent the membrane pore structure, a network of 12 nodes in the x , y and z direction was built [23–25] and an average, constant pore length was assumed [23–26]. To simulate changes in the membrane thickness the authors changed the number of nodes in the direction of the flux, z [24].

The structural network models use the kinetic theory of gasses in order to describe the flux in the system. The fundamental difference in these models is the ability to simulate the topology of the membrane, as well as to apply the proper transport mechanism for each pore, depending on the operating conditions and the pore

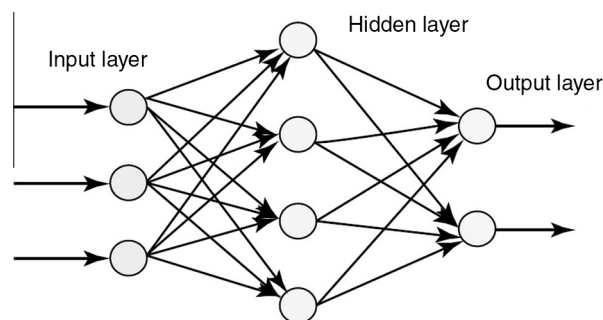


Fig. 6. Multilayered artificial neural network with a single input, output and hidden layer (Ajith [73]).

size. Using the pore size probability density of a real [26] or hypothetical [23–25] membrane and an average pore length, the models are able to map the pore size distribution of the membrane to a 3D network of pores, that connect to each other forming nodes. In order to determine what the governing mass transport mechanism is, the Knudsen number is calculated for each pore based on the temperature, pressure and pore size. If the Knudsen number is larger than one, only Knudsen diffusion would take place. However, if the Knudsen number is smaller than unity, viscous flow would be used to calculate the flux through the pore. To evaluate the pressure drop that drives the viscous flow mechanism, Imdakm and Matsuura [23] assume that the solutions are thoroughly degassed implying that the difference in partial pressure of the water vapour, calculated with the Antoine equation is in fact the total pressure difference.

The SNM models could in theory include molecular diffusion and surface diffusion if needed, however in all of the related articles to date [23–26] the contribution of these transport mechanisms has not been included.

2.3.9. Ballistic transport model

The ballistic transport model is typically used to simulate the motion of electrons in media which has a characteristic size that is smaller than the mean free path of electrons. Soukane et al. [72] used the fact that under the low pressures applied in vacuum membrane distillation, the mean free path of the molecule is also much larger than the pore size (Knudsen type of flow, $Kn > 1$) and applied the ballistic transport model to simulate the fluxes in 8 PVDF membranes. What is unique to this model is that it can split and predict the direct flux contribution of molecules travelling from the pore inlet to the pore outlet without a collision and indirect contribution fluxes where the molecules collide with the pore walls during the transport. Moreover, the model is aimed at predicting the flux at extremely high and extremely low pore length to diameter ratios. The simulation could not predict the flux accurately for all of the membranes and in some cases the relative error of measured and predicted flux was as high as 73%. However, it should be noted that the Knudsen equation prediction was even worse and overall the ballistic transport model was able to fit the data for most of the membranes much better. This model is more complex, but also scientifically significant due to the fact that the flux in a Knudsen type of flow can be predicted in more physical way.

2.4. Empirical models

These models are completely data driven and the underlying equations represent only the final model output and not the actual physical phenomena that occur in the system. Two types of empirical models have been applied to membrane distillation – artificial

neural networks and models derived from the design of experiments toolbox. The empirical models need large amount of data in order to be calibrated, and the output that they generate can only be applied for optimization of the operational conditions, for control strategies and for visualization of the operational space only for the experimental equipment that was used for the model calibration. These models cannot extrapolate outside of the calibration range and cannot be applied to other systems.

2.4.1. Artificial neural network (ANN) models

ANN are designed in a way that mimics the behaviour of biological neural networks. They are organized in a layered structure, where the first and the last layers are the input and output layers and the layers in between are called hidden layers because they are not directly visible to the user. An example layout of an artificial neural network is shown in Fig. 6.

Each circle in Fig. 6 represents a neuron, also called a node which is the building block of the network. The neurons are the basic processing units and each of them consists of a sum and a transfer function.

The configuration of an ANN network can vary greatly, but mostly the model performance is tuned by altering the number of layers and neurons in the hidden layer. By setting a large number of neurons in the hidden layer, the model will likely be able to represent the training data well, however a possibility exists that it will become unable to represent data outside of the training range [73], similarly to a conventional model which is overparameterized. A small number of neurons in the hidden layer will likely not be able to achieve the desired accuracy [73]. Once the ANN network is built it must be trained to represent a given data set. The training process could be supervised, unsupervised or by reinforcement learning. More detailed information about ANN models is available elsewhere [73].

Artificial neural networks are considered as completely black box models, because the mathematical equations in these models are hidden to the modeller and have no physical meaning. They can be used as universal function approximators, even for piecewise and non-linear functions [74]. Khayet and Cojocaru [75,76] published two papers using artificial neural network models for MD.

The first model in 2012 simulated air gap MD and is based on a total of 72 experiments split into 54 for training, 12 for validation and 6 for testing using a network with 10 neurons in the hidden layer [75]. The training and validation points are used during the learning process, whereas the testing points are used to evaluate the model's predictive power subsequent to the learning process. It was concluded that the maximal flux was at the smallest air gap distance, highest feed temperature and flow rate and lowest coolant temperature. The model's predictive power was evaluated based on statistical tests and proved to be high.

The second model using ANN is based on 53 sweep gas MD experiments in total, that were split in the ratio of 41:6:6 for training, validation and testing [76]. The model had 9 neurons in the hidden layer. Similar to the previous model, the optimal operation conditions (maximal flux) were found at the extremes with maximum air and feed flow rates, with the exception of the optimal feed temperature which was 1 degree less than the maximum tested. This model also revealed an interaction between the air gap thickness and the feed flow rate – at large gap thickness the increase of flow rate improved the performance index, while at small gap thickness it had the opposite effect [75]. A similar behaviour was found for the flux as a function of the gap thickness and the inlet temperature of the coolant. The model developed for the sweep gas system also revealed interaction between the sweep gas velocity and the feed inlet velocity [76]. In both models the system optimum was found using the Monte Carlo method [75,76].

2.4.2. Empirical models based on tools from Design of Experiments (DoE)

In conventional experiments one of the degrees of freedom is changed, while the other parameters are kept constant in order to evaluate the impact on the system performance. In a design of experiments the input parameters are changed simultaneously, which reduces the number of experiments and often reveals complex interaction between the system parameters, which are kept hidden using conventional experiments.

Factorial design is a technique where each input parameter is changed in steps, called levels and a low order polynomial is fit as an approximation of the relation of the experimental response and the independent variables [77]. These statistical models are not mechanistic in nature, however the resulting equations can be examined mathematically, so they are not completely black box models as the ANN. A commonly used visualization technique is the Response Surface Methodology (RSM), where the predicted response is plotted in 3D as a function of two of the inputs, that allows to visualize interactions between them. It should be noted that the polynomial fit needs to be an adequate representation of the experimental response in order to have a useful RSM model [77].

Factorial design and RSM models were applied for DCMD by Khayet et al. [78] to optimize the flux by changing the flow rates, mean temperature and initial salt concentrations. The simulations were performed for four different membranes and the model predictions were evaluated as satisfactory when compared to the experimental ones using the coefficient of determination R^2 .

Onsekizoglu et al. applied factorial design and RSM to model the behaviour of flux and dissolved solid content after membrane distillation and osmotic membrane distillation [79] as a function of osmotic agent concentration, flow rates and temperature differences between the feed and the permeate.

Mohammadi and Safavi [80] used the Taguchi method to optimize the performance of vacuum membrane distillation. The Taguchi method is an advanced DoE technique that minimizes the amount of experiments needed for the modelling. The parameters chosen for flux optimization were the different feed flow rates and temperatures, vacuum pressures and inlet concentrations.

Khayet et al. [81] applied factorial design and RSM to optimize the flux of a sweep gas MD system. The operational parameters that were changed are the water and sweep gas inlet temperatures and circulation velocities.

2.5. Computational Fluid Dynamics (CFD) models

Traditionally, the Nusselt and Sherwood equations are used to predict the temperature and concentration at the membrane surface. This approach is semi-empirical and the predicted temperatures and concentrations are uniform. Moreover, these equations are designed for a certain geometry and flow rate regime and the models cannot be reliably used for geometry optimizations.

Computational fluid dynamics uses a numerical approach to simulate a fluid flow. The development of CFD models began in the early 1950s mainly driven by aeronautic problems [82]. The CFD models can be used for virtual geometry prototyping [82]. Moreover, the CFD models for MD can predict the temperatures and concentrations locally throughout the module and can be used for identification of "performance bottlenecks". These models are discussed in more detail, because currently only a few CFD articles exists in the literature and we believe that the MD community will benefit from more CFD studies.

This section is split in three parts. In Section 2.5.1 the models are focusing only on improving the hydrodynamics and heat transfer in the channels of MD. The models in Section 2.5.2 are aimed at improving the flux of the system, but the mass transfer through the

membrane is not directly simulated – instead a constant mass transfer coefficient is given for the membrane across the whole geometry. In the last Section 2.5.3 the models are also simulating the mass transfer across the membrane based on a semi-empirical model.

2.5.1. CFD models for heat transfer optimization in the channels

These types of models focus only on the heat transfer in the channels of the MD module. In order to simulate the process a constant heat flux is imposed at the inner boundaries of a single channel [83,84], or a membrane with a constant thermal conductivity is placed between two flow channels [15]. These models do not account for the flux in the system and are only focused on improving the hydrodynamic conditions and heat transfer in the module channels. Concentration polarization effects are neglected.

Al-Sharif et al. [83] created a 3D model in the open source CFD package Open Foam. Three types of spacers – 90°, 45° and 3 layer double ladder shaped non-woven spacers were simulated and the model was set up assuming a constant heat flux through the membrane in a single channel. Interesting results were obtained concerning the heat transfer improvement by the 3 layer, double ladder spacer. It proved to be the best performing spacer with the least pressure drop. The authors explained that the good performance was due to the flow being forced to go around the middle filament and towards the membrane, thus improving the heat transfer. The heat transfer in the polymer fibres of the spacers was neglected, which could have an impact due to the different heat conductivities of water and polymer. The model was not validated with experimental data.

A three dimensional study of a single feed channel with a 45 degree non-woven spacer was published by Cipollina et al. [84]. A constant negative heat flux was imposed in order to simulate 5 kg/(m² h) vapour flux through the membrane. The simulation was done at a Reynolds number of 91 and the conductivity of the spacer material was neglected. The model was tested for mesh dependency, but was not validated with experimental data.

A two dimensional CFD model was simulated by Shakaib et al. [15] in the commercial CFD software Fluent (Ansys). The model was set up with two channels (feed and permeate) that were flowing around a single flat sheet membrane in counter current fashion. The thermal conductivity of the membrane material was set to a constant value of 0.2 W/(m² K). The conductive heat transfer in the spacer material was included in the calculation. The authors state that when the maximum velocity in the channels exceeded 0.15 m/s (Re number 350) the model failed to converge with Navier–Stokes equations and they used the Spalart–Allmaras turbulence model. Different 90° spacer arrangements were tested with the spacer filaments adjacent to the membrane, away from the membrane and a staggered (alternating) configuration. The performance of the spacers was evaluated based on the temperature polarization coefficient and the pressure drop in the channels. The model was tested for grid size dependency and there was no change of the simulated results with a higher number of grid cells. The Nusselt numbers that described the heat transfer in the simulation were compared to those obtained in the experimental work of Phattaranawik et al. [8]. The general trend was the same between the results from different arrangements and spacer channels and conventional Nusselt equation, but a direct comparison could not be made due to insufficient information on the exact experimental details.

2.5.2. CFD models for heat and mass transfer optimization in the channels

A series of articles was published by Yu et al. [12,13] and Yang et al. [10,11] focusing on the simulation of heat flow and hydrodynamics inside a hollow fibre module with a single membrane. The

simulations focused on module design and a constant membrane distillation coefficient was used to estimate the flux. The MD coefficient is usually expressed in units kg/(m² s bar) and has the physical meaning of flux per intermembrane water vapour pressure difference. The models were set up with laminar flow when Reynolds numbers were ranging were 200–2000 and with $k - \epsilon$ turbulence model when this range was exceeded or turbulence promoters were used [10,11]. The flux influence on the heat transfer was included in the form of latent heat of evaporation but was neglected hydrodynamically [10,12,13], because of being 3 orders of magnitude lower than the feed flow rate [12]. The group published 3 articles arranged in 2D [10,12,13] and one article in 3D [11]. The first article by Yu et al. [12] studied a single straight hollow fibre membrane and cylindrical shell side of the module. The study was focused on local fluxes, and heat flows, energy efficiencies and temperature polarization coefficients. The outlet temperatures were compared to experimental data at different module lengths in order to validate the model, revealing less than 1 percent error in the prediction.

The second article in the sequence by Yu et al. [13], extended the previous one by including baffles on the sides of the hollow fibre module. This simulation was again performed with a constant membrane MD coefficient. The influence of the MD coefficient on the temperature polarization coefficient was studied. It was concluded that turbulence promoters are an important tool for flux increase especially when membranes with a high MD coefficient were used. It was found that at high operating temperatures the energy efficiency of the process is substantially increased, even at small temperature differences between the feed and permeate. The obtained fluxes were compared to experimental results and showed excellent correlation.

The work of Yu et al. [12,13] was extended by Yang et al. [10] by including different spacers attached to a single hollow fibre membrane in combination with baffles on the shell side of the module. The effect of turbulence promoters on energy efficiency improvement was found to be less than 5 percent in the tested conditions. The best compromise between hydraulic energy consumption and flux improvement was achieved with the floating round spacers and with the attached quad (square shaped) spacers. The model was validated by comparing simulated fluxes with the experimental ones at fixed inlet temperatures with the different geometries. The validation showed an excellent correlation with errors in the mass fluxes being less than 5 percent.

The last article in the sequence by Yang et al. [11] used a 3D geometry, further expanding the previous 2D models. The tested geometries included hollow fibre membranes with wavy and gear-shaped outer surfaces. The constant MD coefficient assumption was maintained. Only the gear-shaped membrane was given a slightly lower MD coefficient to account for the cross sections that had a higher thickness. The model was not validated, based on the concept that the previous 2D based models are valid.

2.5.3. CFD system models including the mass transfer inside the membrane

Charfi et al. [85] developed a two dimensional numerical model for the simulation of sweeping gas membrane distillation. This MD configuration uses a sweeping gas to lower the partial pressure of water vapours on the permeate side and later the gas is regenerated in an external condenser. The geometry was limited to a flat sheet membrane with empty channels (without spacers). The system was based on the Navier–Stokes equation coupled with the Darcy–Brinkman–Forschheimer formulation in transient regime for the porous partition. The model was able to simulate different changes in water and sweep gas velocities and compared the results to experimental data with a relatively good fit.

Table 4

Overview of the different models available in the literature.

| System definition | Model type | Strengths | Weaknesses | Remarks and gaps |
|-------------------------------|--|--|--|---|
| Heat transfer in the channels | Nusselt-based | Simple, low computational burden | Single, uniform interfacial temperature is predicted | In some studies the calibration is not properly performed |
| | Computational fluid dynamics | Mechanistic approach. Temperature field is predicted | High computational burden | Commonly the geometry is over-simplified, HT in spacer material often excluded; Turbulence models are used for very low (laminar) flow velocities |
| Mass transfer in the channels | Sherwood-based | Simple, low computational burden | Single uniform interfacial concentration is predicted | Validation is missing |
| | Computational fluid dynamics | Mechanistic approach, concentration field is predicted | High computational burden | No models exist so far |
| Heat transfer in the membrane | Isostress, Isostrain, other | Simple, low computational burden | | Validation is missing; unclear which model works best |
| Mass transfer in membrane | Dusty gas model | Good prediction, low computational burden | Lumped membrane properties | Accepted by the community, regarded as mechanistic |
| | Schofield's | Simple, low computational burden | Difficult to evaluate membrane parameters experimentally | Not widely used; Sometimes referred "less physical" than the DGM |
| | Pore size distribution models | More mechanistic | Complexity | Pore size distribution effect is assumed small; few articles in the literature |
| | Structural network model | Mechanistic; Simulates membrane structure | Complexity, high computational burden | Only used by one group; Excludes molecular diffusion, constant pore size and membrane thickness; Too small structure to be representative |
| | Ballistic transport model | Mechanistic; Can predict the flux in extremely short or long pores | High complexity and computational burden | Only one article; not fully tested |
| | Surface diffusion | | | Not included in any membrane model so far |
| Overall system models | Artificial neural network | Can behave similarly to real system; Low computational burden | Black-box models; Large amount of experimental data needed | Cannot be used for extrapolation beyond the calibration range |
| | Design of experiments-based | Simple, low computational burden | Non-mechanistic models | Cannot be used for extrapolation beyond the calibration range |
| | Nusselt and Sherwood eqns. and membrane MT model | Simple, low computational burden | Semi-empirical | Uniform prediction for temperature and concentration, not suitable for proper module design |
| | Computational fluid dynamics | The most mechanistic approach | High computational burden | Commonly oversimplified in terms of physics and geometry; Validation sometimes missing |

Another CFD study by Xu et al. [86] incorporated the Knudsen-viscous transition of the DGM to simulate an air-gap MD system. The authors set up a two-dimensional axisymmetric model of a single hollow fibre. The effect of vapour pressure reduction due to activity was taken into account, however the feed concentration of NaCl was set quite low at 0.2 wt%. The concentration polarization as well as thermal conduction through the membrane were neglected. The $k-\epsilon$ turbulence model was chosen to simulate the water flowing inside the module at Reynolds numbers between 3400 and 10,200. The model dependency on the feed temperature and flow rate was validated by comparison with experimental fluxes and showed excellent correlation. However, we must state that the validation of the feed flow rate was done in a region where the flux was nearly independent on the flow rate and was almost constant. Exact details on how the simulation was set up are missing.

Hwang et al. [87] developed a model that included the mass transfer inside the membrane using the commercial CFD software COMSOL. The geometry of a single flat sheet PTFE membrane was modelled for a lab-scale (0.06 m^2) rectangular module and fluid velocities of 0.17–0.55 m/s. The authors calculated a local flux via the local vapour pressure difference and the membrane MD coefficient. The MD coefficient was also calculated locally using the dusty gas model throughout the membrane length. Attention was given to the choice of flow configuration (short or long side) of the module in co- and countercurrent operation. The average and local vapour pressure was studied, and also the feed concentration of NaCl was varied from 1 to 6%. The model was validated by comparison of the experimental and simulated fluxes, as well as outlet

temperature comparison, showing excellent prediction of the model. Exact details on how the simulations were set up are missing.

3. Discussion and research gaps

There are different models and submodels that could be used in MD and in order to orient the reader what information could be reliably delivered from each type of model, we are classifying them into 4 categories: Process understanding and optimization, module design, process control and membrane synthesis.

The process understanding and optimization models are usually based on a combination between the Nusselt and Sherwood equations for the heat and mass transfer in the channels together with a mass transfer model for the membrane (see Table 4). In order to simulate the mass transfer for the membrane, we would recommend the use of the dusty gas model, because of the more physical approach compared to the Schofield's.

CFD could be used for module design in order to investigate the local temperature and concentration polarization, flux and pressure drop in lab-scale modules. CFD can also aid the design of novel spacers that lead to a better mixing performance and lower pressure drop.

The empirical models based on ANN and RSM could be used to visualize the operational space and help understand the system behaviour. These models can be implemented in process control models, but cannot be used to explain the physical phenomena or to extrapolate the results to another system.

The dusty gas model using the extension for pore size distribution, the structural network models and the ballistic transport models can be used for better understanding of the mass transfer inside the membrane and to apply the knowledge for better membrane synthesis.

A summary of the models is given in Table 4.

3.1. Discussion

Most of the modelling efforts of heat transfer in MD literature is based on various Nusselt equations. They can predict the average interfacial temperatures with satisfactory accuracy as recently shown by Ali et al. [2] and Tamburini et al. [3,4]. However, special care should be taken when choosing the appropriate Nusselt equation for the given geometry and flow regime. When modelling the system, it is important to first perform heat transfer experiments to validate the choice of Nusselt equation (as described in Section 2.1.4), otherwise the heat transfer could be over or underestimated by orders of magnitude. Often the heat transfer models are not validated separately, but the performance of the whole model (heat and mass transfer) is validated by comparison of the predicted and measured fluxes. This could lead to an error of the mass transfer model being compensated by the error of the heat transfer model and an overall predictive power for only a very small range of temperatures and flow rates.

CFD has also been used to simulate the temperature polarization effect in the channels of MD [15,83]. The advantage of CFD simulations over Nusselt equation type models is that a field of temperature can be predicted, and therefore the performance of different spacers and module configurations can be accessed. However, CFD models are associated with very large computational burden.

The concentration polarization effects are commonly simulated with the Sherwood equation. By recognizing the analogy between heat and mass transfer, most MD authors use the same form of the Sherwood equation as the Nusselt equation they used for the heat transfer model. This approach has not been validated by direct experiments.

Numerous models have been developed based on the DGM to describe the mass transfer inside the membrane. It has been widely accepted in the MD community and describes the system with satisfactory accuracy. Recent critique of the DGM was published by Field et al. [68], concerning the parallel addition of Knudsen and viscous flux and some modifications have been proposed by the authors for the flux calculation in the Knudsen-molecular transition region. However, more work is needed to test the validity of this new extension.

The model proposed by Schofield et al. [21,22] could also be used to simulate the mass transfer in the membrane, however it is not widely used in the MD community. It has been criticized by Lawson and Lloyd [19] and Fernandez et al. [46] for having large experimental error associated with the gas permeation calibration experiments. Fernandez et al. [46] concluded that the DGM is more physically sound compared to Schofield's model.

Pore size distribution models have been developed based on the KTG for cylindrical pores by Khayet et al. [9] and the DGM by Phattaranawik et al. [69]. The models were able to estimate the effect of pore size distribution on MD performance. Both authors concluded that this influence is relatively small, especially for commercial membranes [9], where the pore size distribution is usually very narrow.

A series of structural pore network models has been published by Imdakm [23–25] and Khayet et al. [26]. The approach of the authors represents a network of nodes interconnected by pores and a combination of viscous and Knudsen flow is used to calculate the flux based on the Knudsen number. The key aspect of these

models is the ability to simulate the effect of membrane structure. Although the authors claim that molecular diffusion could be included in the model structure, so far such model does not exist. These models are computationally intensive and complex, and have not yet been further used by the MD community.

The ballistic transport model was applied to simulate Knudsen flow by Soukane et al. [72]. This model has the advantage that it can predict the flux of water vapour at very high and very low pore length to diameter ratios. It is burdened with high complexity and computational requirements, but it is scientifically significant due to its novel and mechanistic approach.

Artificial neural network models were used to simulate different configurations of MD [75,76]. The models could represent the behaviour of the system and reveal complex interactions between the input parameters. The ANN models have the disadvantage that a large number of experimental runs must be performed for training, validation and testing and are only applicable to the experimental system that they are trained for. Moreover, these types of models are considered as a complete black box and non-mechanistic.

Models from the Design of Experiments toolbox were used to simulate various MD configurations by Khayet et al. and Onsekizoglu et al. [78,79,81]. These models were able to reveal interactions between the input parameters of the system similarly to ANN. They are non-mechanistic in their nature but can help building the mechanistic knowledge base. They also have the benefit of allowing statistical assessments. Care should be taken that the predictions of these models are properly tested for statistical significance before they are used to optimize the system.

Most authors of CFD system models assume that the MD coefficient is constant for a narrow temperature range as commonly quoted in the MD literature [12,48,68,70]. Although the change of membrane permeability with temperature is small (estimated to be within 3 percent for every 10 °C [48]), the calculation of the local permeability coefficient is not computationally intensive and therefore a better approach to use in the CFD model, which is done so far only by a few authors [85–87].

Many authors use turbulent models in their CFD simulations [10,11,15,88]. Turbulence models are needed in order to approximate the behaviour of turbulent flows, which is otherwise prohibitively expensive to solve directly in terms of computational power. The flow inside spacer filled channels (commonly used in MD) is rarely fully turbulent [89] and the simulation of the transition between laminar and fully turbulent flow is extremely challenging as Nichols points out [90]. Fimbres-Weihs and Wiley [89] reports in their review that the Reynolds numbers typically encountered in spacer filled channels are between 1000 and 3000. Moreover, the authors state that turbulence models can only be properly used at Re numbers above 30,000 when the flow is fully turbulent [89]. We therefore believe that if turbulent models are used, they must always be checked for validity against experimental data. The work of Tamburini et al. [3,4] could be used for CFD model calibration and validation of heat transfer in spacer filled channels.

3.2. Research gaps

Although a lot of good models exist in the literature, more work needs to be done in the area of module design. Until recently, MD modules only have been modelled based on the semi-empirical Nusselt and Sherwood equations. Recent attempts on module design have been made to simulate the system with CFD, however often times either the geometry, or the physical phenomena are oversimplified. We believe that proper CFD based module design is key in order to make MD a competitive separation technology

and more effort has to be put into the design of modules specifically optimized for MD.

The advantage of CFD studies over Sherwood equation mass transfer models is that the “hot spots” of concentration polarization can be identified and optimized in order to minimize the concentration polarization effects and possibly avoid membrane scaling in complex geometries such as spacer filled channels. However, so far such studies do not exist in the literature. Moreover, no study to date includes the influence of the convective flow near the membrane driven by the flux. Although this convective flow is expected to be several orders of magnitude smaller than the bulk flow [12], it is located in the stagnant boundary layer near the membrane surface and could have a significant interaction with the other phenomena that occur in the module. In fact, this flow is the sole driving force of the concentration polarization.

The CFD studies regarding the heat transfer in MD have received more attention. However, the studies on spacer-filled channels are oversimplified and only take into account the heat transfer of the system. In the current CFD models of hollow fibre modules the geometry is simplified to a single membrane inside a shell [10–13,88]. The interaction effects between randomly packed hollow fibres could be tackled analytically [91,92] by drawing straight lines at equal distances between each randomly packed membrane, forming a polygonal structure around the fibre [93] called Voronoi tessellation. However, the interaction effect between the fibres so far has not been studied via CFD modelling.

The energy efficiency is an important parameter, essential to the industrial application of MD, but it is not always included in experimental and modelling articles. In order to calculate the energy efficiency, the thermal conductivity of the membrane matrix must be calculated, but it is still unclear which is the best performing equation. The experimental evaluation of this parameter is not trivial because it is based on clamping the material between solid discs [33], and some authors argue that the porous membrane can be compressed during these tests [29]. An evaluation of the thermal conductivity with a less invasive experimental method could be very beneficial for modelling purposes.

Multiple models exist in the literature to calculate the mass transfer for the membrane region, but some gaps still exist in this field. The structural network models that can be used in MD for flux evaluation includes 12 nodes in each axis direction [23–25] and uses pore lengths of 1 μm . Accounting for the fact that each node has two pores in each direction the resulting membrane thickness is 24 μm [23–25]. It would be interesting to see the effect of changing the membrane pore length, which is not shown in any of the structural network models – and possibly to use a pore length distribution rather than a uniform, constant length of 1 μm . Moreover, the studies so far account for only 12 nodes in each direction, resulting in only about 5200 pores. It would be beneficial to show models with more pores and evaluate if this has an effect on the system performance. The current SNM models for MD exclude the influence of molecular diffusion and instead it is replaced by viscous flow. A SNM model which includes the influence of molecular diffusion would be valuable to the MD community.

The surface diffusion transport mechanism inside the membrane has always been neglected in MD modelling, relying on the assumption that the membranes are hydrophobic and the interaction between the water vapour molecules and the surface of the membrane will be low. However, many membranes used in MD are only slightly hydrophobic (e.g. PVDF) and the contribution of this transport mechanism might not be negligible. Hence, the simulation results could be beneficial for membrane synthesis.

Most of the studies have not been extensively calibrated. In many of the models the tortuosity is manually adjusted and used as a tuning parameter and the use of special calibration tools

applied to a MD model is lacking. Moreover, sensitivity analyses for the model parameters as well as the operational conditions is performed on only a few models [70,93–95] and should be explored in more detail.

4. Conclusions

Membrane distillation has been discovered 50 years ago, but so far lacks significant industrial applications. In order to optimize the technology and make it competitive to alternative separation techniques the MD community must have an in-depth understanding of the processes that occur inside the modules and the membranes.

The mass transfer modelling of the membrane region has been covered by many different mechanistic and statistical models that can predict the flux with varying accuracy. More recent models such as the ballistic transport model and the structural network models are innovative and interesting to the community, but have not yet been thoroughly tested and validated. Moreover, some of the physical phenomena that occur inside the membrane such as the surface diffusion has always been neglected in MD modelling which can prove to be important for membrane synthesis studies.

We believe that the lack of significant industrial applications of the technology is also due to the lack of proper module design, for which CFD can be helpful. Some of the recent CFD studies have focused on this task, however in most of the cases either the physical phenomena or the geometry have been severely oversimplified, leaving a room for further research.

References

- [1] B.R. Bodel, Silicone Rubber Vapor Diffusion in Saline Water Distillation, United States Patent Serial No. 285,032, 1963.
- [2] A. Ali, F. Macedonio, E. Drioli, O. Aljlil, S. Alharbi, Experimental and theoretical evaluation of temperature polarization phenomenon in direct contact membrane distillation, *Chem. Eng. Res. Des.* 91 (2013) 1966–1977.
- [3] A. Tamburini, G. Micale, M. Ciofalo, A. Cipollina, Experimental analysis via thermochromic liquid crystals of the temperature local distribution in membrane distillation modules, *Chem. Eng. Trans.* 32 (2013) 2041–2046.
- [4] A. Tamburini, P. Pitò, A. Cipollina, G. Micale, M. Ciofalo, A thermochromic liquid crystals image analysis technique to investigate temperature polarization in spacer – filled channels for membrane distillation, *J. Membrane Sci.* 447 (2013) 260–273.
- [5] V.U. Kakade, M. Lock, G.D. Wilson, J.M. Owen, J. Mayhew, Accurate heat transfer measurements using thermochromic liquid crystal. Part 1: calibration and characteristics of crystals, *Int. J. Heat Fluid Flow* 30 (2009) 939–949.
- [6] M. Gryta, M. Tomaszewska, M.A. Morawski, Membrane distillation with laminar flow, *Sep. Purif. Technol.* 11 (1997) 93–101.
- [7] M. Gryta, M. Tomaszewska, Heat transport in the membrane distillation process, *J. Membrane Sci.* 144 (1998) 211–222.
- [8] J. Phattaranawik, R. Jiraratananon, A. Fane, Heat transport and membrane distillation coefficients in direct contact membrane distillation, *J. Membrane Sci.* 212 (2003) 177–193.
- [9] M. Khayet, A. Velazquez, J. Mengual, Modelling mass transport through a porous partition: effect of pore size distribution, *J. Non-Equil. Thermody.* 29 (2004) 279–299.
- [10] X. Yang, H. Yu, R. Wang, A.G. Fane, Analysis of the effect of turbulence promoters in hollow fiber membrane distillation modules by computational fluid dynamics (CFD) simulations, *J. Membrane Sci.* 415–416 (2012) 758–769.
- [11] X. Yang, H. Yu, R. Wang, A.G. Fane, Optimization of microstructured hollow fiber design for membrane distillation applications using CFD modelling, *J. Membrane Sci.* 421–422 (2012) 258–270.
- [12] H. Yu, X. Yang, R. Wang, A.G. Fane, Numerical simulation of heat and mass transfer in direct membrane distillation in a hollow fiber module with laminar flow, *J. Membrane Sci.* 384 (2011) 107–116.
- [13] H. Yu, X. Yang, R. Wang, A.G. Fane, Analysis of heat and mass transfer by CFD for performance enhancement in direct contact membrane distillation, *J. Membrane Sci.* 405–406 (2012) 38–47.
- [14] M. Shakaib, A. Iqbal, R.M. Yunus, CFD modeling for fluid flow and heat transfer in membrane distillation, in: 2nd International Conference on Environmental Science and Technology, 2011, pp. 265–268.
- [15] M. Shakaib, S. Hasani, I. Ahmed, R.M. Yunus, A CFD study on the effect of spacer orientation on temperature polarization in membrane distillation modules, *Desalination* 284 (2012) 332–340.
- [16] M. Khayet, Membranes and theoretical modeling of membrane distillation: a review, *Adv. Colloid. Interfac.* 164 (2011) 56–88.
- [17] F. Lagana, G. Barbieri, E. Drioli, Direct contact membrane distillation: modelling and concentration experiments, *J. Membrane Sci.* 166 (2000) 1–11.

- [18] K.W. Lawson, D.R. Lloyd, Membrane distillation. II. Direct contact MD, *J. Membrane Sci.* 120 (1996) 123–133.
- [19] K.W. Lawson, D.R. Lloyd, Membrane distillation, *J. Membrane Sci.* 124 (1997) 1–25.
- [20] L. Martínez, J. Rodríguez-Maroto, On transport resistances in direct contact membrane distillation, *J. Membrane Sci.* 295 (2007) 28–39.
- [21] R.W. Schofield, A.G. Fane, C.J.D. Fell, Gas and vapor transport through microporous membranes. I. Knudsen–Poiseuille transition, *J. Membrane Sci.* 53 (1990) 159–171.
- [22] R.W. Schofield, A.G. Fane, C.J.D. Fell, Gas and vapor transport through microporous membranes. II. Membrane distillation, *J. Membrane Sci.* 53 (1990) 173–185.
- [23] A. Imdakm, T. Matsuura, A monte carlo simulation model for membrane distillation process: direct contact (MD), *J. Membrane Sci.* 237 (2004) 51–59.
- [24] A. Imdakm, T. Matsuura, Simulation of heat and mass transfer in direct contact membrane distillation (MD): the effect of membrane physical properties, *J. Membrane Sci.* 262 (2005) 117–128.
- [25] A. Imdakm, M. Khayet, T. Matsuura, A monte carlo simulation model for vacuum membrane distillation process, *J. Membrane Sci.* 306 (2007) 341–348.
- [26] M. Khayet, A. Imdakm, T. Matsuura, Monte carlo simulation and experimental heat and mass transfer in direct contact membrane distillation, *Int. J. Heat Mass Tran.* 53 (2010) 1249–1259.
- [27] M. Qtaishat, T. Matsuura, B. Krucek, M. Khayet, Heat and mass transfer analysis in direct contact membrane distillation, *Desalination* 219 (2008) 272–292.
- [28] E. Curcio, E. Drioli, Membrane distillation and related operations – a review, *Separ. Purif. Rev.* 34 (2005) 35–86.
- [29] J. Zhang, S. Gray, J. Li, Modelling heat and mass transfers in DCMD using compressible membranes, *J. Membrane Sci.* 387–388 (2012) 7–16.
- [30] K.K. Sirkar, L. Song, Pilot-scale studies for direct contact membrane distillation-based desalination process, US Department of the Interior Bureau of Reclamation, Report No. 134, 2009. <<http://www.usbr.gov/research/AWT/reportpdfs/report134.pdf>>.
- [31] L. Martínez-Díez, M. Vázquez-González, F.J. Florido-Díaz, Study of membrane distillation using channel spacers, *J. Membrane Sci.* 144 (1998) 45–56.
- [32] A. Jonsson, R. Wimmerstedt, A. Harrysson, Membrane distillation – a theoretical study of evaporation through microporous membranes, *Desalination* 56 (1985) 237–249.
- [33] M.C. García-Payo, M.A. Izquierdo-Gil, Thermal resistance technique for measuring the thermal conductivity of thin microporous membranes, *J. Phys. D* 37 (21) (2004) 3008–3016.
- [34] L.F. Dumée, S. Grey, M. Duke, K. Sears, J. Schültz, N. Finn, The role of membrane surface energy on direct contact membrane distillation performance, *Desalination* 323 (2013) 22–30.
- [35] M. Izquierdo-Gil, M. García-Payo, C. Fernandez-Pineda, Air gap membrane distillation of sucrose aqueous solutions, *J. Membrane Sci.* 155 (1999) 291–307.
- [36] A. Bahmanyar, M. Asgharia, N. Khoobi, Numerical simulation and theoretical study on simultaneously effects of operating parameters in direct contact membrane distillation, *Chem. Eng. Process.* 61 (2012) 42–50.
- [37] A. Saleem, L. Frommann, A. Iqbal, High performance thermoplastic composites: Study on the mechanical, thermal, and electrical resistivity properties of carbon fiber-reinforced polyetheretherketone and polyethersulphone, *Polym. Compos.* 28 (2007) 785–796.
- [38] L. Martínez-Díez, Vázquez-González, Temperature and concentration polarization in membrane distillation of aqueous salt solutions, *J. Membrane Sci.* 156 (1999) 265–273.
- [39] M.N. Chernishov, G.W. Meindersma, A.B. de Haan, Modelling of temperature and salt concentration distribution in membrane distillation feed channel, *Desalination* 157 (2003) 315–324.
- [40] M. Gryta, Fouling in direct contact membrane distillation process, *J. Membrane Sci.* 325 (2008) 383–394.
- [41] S. Srisurichan, R. Jiraratananon, A. Fane, Mass transfer mechanisms and transport resistances in direct contact membrane distillation process, *J. Membrane Sci.* 277 (2006) 186–194.
- [42] Y. Yun, R. Ma, W. Zhang, A.G. Fane, J. Li, Direct contact membrane distillation mechanism for high concentration nacl solutions, *Desalination* 188 (2006) 251–262.
- [43] J. Gilron, Y. Ladizansky, E. Korin, Silica fouling in direct contact membrane distillation, *Ind. Eng. Chem. Res.* 52 (2013) 10521–10529.
- [44] J.W. Chew, W.B. Krantz, A.G. Fane, Effect of a macromolecular- or bio-fouling layer on membrane distillation, *J. Membrane Sci.* 456 (2014) 66–76.
- [45] L. Martínez, F. Florido-Díaz, Theoretical and experimental studies on desalination using membrane distillation, *Desalination* 139 (2001) 373–379.
- [46] C. Fernández-Pineda, M.A. Izquierdo-Gil, M.C. García-Payo, Gas permeation and direct contact membrane distillation experiments and their analysis using different models, *J. Membrane Sci.* 198 (1) (2002) 33–49.
- [47] A. Sereno, M. Hubinger, J. Comesana, A. Correa, Prediction of water activity of osmotic solutions, *J. Food. Eng.* 49 (2011) 103–114.
- [48] R. Schofield, A. Fane, C. Fell, Heat and mass transfer in membrane distillation, *J. Membrane Sci.* 33 (3) (1987) 299–313.
- [49] M. Khayet, T. Matsuura, Membrane Distillation Principles and Applications, Elsevier, 2011.
- [50] A.J.J. Fontana (Ed.), Water Activity in Foods: Fundamentals and Applications, Wiley, 2007 (Appendix B).
- [51] Food, Drug Administration, Bad bug book, foodborne pathogenic microorganisms and natural toxins, second ed., USDA, 2012, (Appendix 3).
- [52] D. Kitic, D.C.P. Jardim, G.J. Favetto, S.M. Resnik, C. Jorge, Theoretical prediction of the water activity of standard saturated salt solutions at various temperatures, *J. Food Sci.* 51 (1986) 1037–1041.
- [53] J. Chirife, S.L. Resnik, Unsaturated solutions of sodium chloride as reference sources of water activity at various temperatures, *J. Food Sci.* 49 (1984) 1486–1488.
- [54] K.S. Pitzer, G. Mayorga, Thermodynamics of electrolytes. ii. Activity and osmotic coefficients for strong electrolytes with one or both ions univalent, *J. Phys. Chem.* 77 (1973) 2300–2308.
- [55] H. Renon, J.M. Prausnitz, Estimation of parameters for the NRTL equation for excess Gibbs energies of strongly nonideal liquid mixtures, *Ind. Eng. Chem. Process. Des. Dev.* 8 (1969) 413–419.
- [56] E. Mason, A. Malinauskas, Gas transport in porous media: the dusty-gas model, in: *Chemical Engineering Monographs*, vol. 17, 1983.
- [57] R. Krishna, Problems and pitfalls in the use formulation for intraparticle of the Fick diffusion, *Chem. Eng. Sci.* 48 (1993) 845–861.
- [58] E. Close, E. Sorensen, Modelling of direct contact membrane distillation for desalination, in: 20th European Symposium on Computer Aided Process Engineering – ESCAPE20, 2010.
- [59] C. Rieckmann, F.J. Keil, Multicomponent diffusion and reaction in three-dimensional networks: general kinetics, *Ind. Eng. Chem. Res.* 36 (8) (1997) 3275–3281.
- [60] M. Matsumoto, K. Yosuke, Study on liquid-vapor interface of water. I. Simulation results of thermodynamic properties and orientational structure, *J. Chem. Phys.* 88 (1988) 3233–3245.
- [61] K.W. Lawson, D.R. Lloyd, Membrane distillation. I. Module design and performance evaluation using vacuum membrane distillation, *J. Membrane Sci.* 120 (1996) 111–121.
- [62] C. Guijt, Rácz, T. Reith, A.B. de Haan, Determination of membrane properties for use in the modelling of a membrane distillation module, *Desalination* 132 (2000) 255–261.
- [63] F. Gao, X. Chen, G. Yu, C. Asumana, Compressible gases transport through porous membrane: a modified dusty gas model, *J. Membrane Sci.* 379 (2011) 200–206.
- [64] Z. Lei, B. Chen, Z. Ding, Membrane distillation, in: *Special Distillation Processes*, Elsevier Science, 2005.
- [65] J. Zhang, Theoretical and Experimental Investigation of Membrane Distillation, Ph.D. Thesis, Victoria University, 2011.
- [66] J. Zhang, J.-D. Li, M. Duke, M. Hoang, Z. Xie, A. Groth, C. Tun, S. Gray, Modelling of vacuum membrane distillation, *J. Membrane Sci.* 434 (2013) 1–9.
- [67] K.W. Lawson, M.S. Hall, D.R. Lloyd, Compaction of microporous membranes used in membrane distillation. I. Effect on gas permeability, *J. Membrane Sci.* 101 (1994) 99–108.
- [68] R.W. Field, H.Y. Wu, J.J. Wu, Multiscale modeling of membrane distillation: Some theoretical considerations, *Ind. Eng. Chem. Res.* 52 (2013) 8822–8828.
- [69] J. Phattaranawik, R. Jiraratananon, A. Fane, Effect of pore size distribution and air flux on mass transport in direct contact membrane distillation, *J. Membrane Sci.* 215 (2003) 75–85.
- [70] R. Schofield, A. Fane, C. Fell, R. Macoun, Factors affecting flux in membrane distillation, *Desalination* 77 (1990) 279–294.
- [71] C.Z. Mooney, Monte Carlo Simulation, vol. 116, SAGE Publications, Inc., 1997.
- [72] S. Soukane, S. Chelouche, M. Naceur, A ballistic transport model for vacuum membrane distillation, *J. Membrane Sci.* 450 (2014) 397–406.
- [73] A. Ajith, Artificial Neural Networks, John Wiley and Sons Ltd, 2005. ISBN 0-470-02143-8.
- [74] T. Hill, L. Marquez, O. Marcus, W. Remus, Artificial neural network models for forecasting and decision making, *Int. J. Forecasting* 10 (1994) 5–15.
- [75] M. Khayet, C. Cojocar, Artificial neural network modelling and optimization of desalination by air gap membrane distillation, *Sep. Purif. Technol.* 86 (2012) 171–182.
- [76] M. Khayet, C. Cojocar, Artificial neural network model for desalination by sweeping gas membrane distillation, *Desalination* 308 (2013) 102–110.
- [77] D.C. Montgomery, Design and Analysis of Experiments, third ed., John Wiley and Sons, 1991.
- [78] M. Khayet, C. Cojocar, C. Garcia-Payo, Application of response surface methodology and experimental design in direct contact membrane distillation, *Ind. Eng. Chem. Res.* 46 (2007) 5673–5685.
- [79] P. Onsekizoglu, K. Savas Bahceci, J. Acar, The use of factorial design for modeling membrane distillation, *J. Membrane Sci.* 349 (2010) 225–230.
- [80] T. Mohammadi, M.A. Safavi, Application of taguchi method in optimization of desalination by vacuum membrane distillation, *Desalination* 249 (2009) 83–89.
- [81] M. Khayet, C. Cojocar, A. Baroudi, Modeling and optimization of sweeping gas membrane distillation, *Desalination* 287 (2012) 159–166.
- [82] J.D. Anderson, G. Degrez, J. Degroote, E. Dick, R. Grundmann, J. Vierendeels, Computational Fluid Dynamics, An Introduction, third ed., Springer, 2009.
- [83] S. Al-Sharif, M. Albeirutty, A. Cipollina, G. Micale, Modelling flow and heat transfer in spacer-filled membrane distillation channels using open source CFD code, *Desalination* 311 (2013) 103–112.
- [84] A. Cipollina, A. Di Miceli, J. Koschikowski, G. Micale, L. Rizzuti, CFD simulation of a membrane distillation module channel, *Desalin. Water Treat.* 6 (2009) 177–183.

- [85] K. Charfi, M. Khayet, M. Safi, Numerical simulation and experimental studies on heat and mass transfer using sweeping gas membrane distillation, *Desalination* 259 (2010) 84–96.
- [86] Z. Xu, Y. Pan, Y. Yu, CFD simulation on membrane distillation of NaCl solution, *Front. Chem. Eng. China* 3 (2009) 293–297.
- [87] H.J. Hwang, K. He, S. Gray, J. Zhang, S. Moon, Direct contact membrane distillation (DCMD): experimental study on the commercial PTFE membrane and modelling, *J. Membrane Sci.* 371 (2011) 90–98.
- [88] N. Tang, H. Zhang, W. Wang, Computational fluid dynamics numerical simulation of vacuum membrane distillation for aqueous NaCl solution, *Desalination* 274 (2011) 120–129.
- [89] G.A. Fimbres-Weihs, D.E. Wiley, Review of 3D CFD modeling of flow and mass transfer in narrow spacer-filled channels in membrane modules, *Chem. Eng. Process* 49 (2010) 759–781.
- [90] R. Nichols, *Turbulence Models and their Application to Complex Flows*, 2012. <http://people.nas.nasa.gov/pulliam/Turbulence/Turbulence_Guide_v4.01.pdf>.
- [91] D. Zhongwei, L. Liying, M. Runyu, Study on the effect of flow maldistribution on the performance of the hollow fiber modules used in membrane distillation, *J. Membrane Sci.* 215 (2013) 11–23.
- [92] V. Chen, M. Hlavacek, Application of voronoi tessellation for modeling randomly packed hollow-fiber bundles, *AIChE J.* 40 (1991) 606–612.
- [93] S. Al-Obaidani, E. Curcio, F. Macedonio, G. Di Profio, H. Al-Hinai, E. Drioli, Potential of membrane distillation in seawater desalination: thermal efficiency, sensitivity study and cost estimation, *J. Membrane Sci.* 323 (2008) 85–98.
- [94] F. Banat, F.A. Al-Rub, K. Bani-Melhem, Desalination by vacuum membrane distillation: sensitivity analysis, *Sep. Purif. Technol.* 33 (2003) 75–87.
- [95] F.A.A. Al-Rub, F. Banat, K. Beni-Melhim, Parametric sensitivity analysis of direct contact membrane distillation, *Sep. Purif. Technol.* 37 (2001) 3245–3271.